Electronic Supplementary Material (ESI) for Polymer Chemistry.

Electronic Supporting Information

for

Simulation of "cold" free radical polymerization of methyl methacrylate using a tertiary amine/BPO initiating system

Alexander Zoller, Didier Gigmes, and Yohann Guillaneuf*

* Corresponding Authors

[a] Aix-Marseille Université, CNRS, ICR UMR 7273, 13397 Marseille, France

Fax: +33 (0)4 91 28 87 58; Tel: +33 (0)4 91 28 28 10; E-mail: yohann.guillaneuf@univ-amu.fr

1. Materials

Dibenzoylperoxide (BPO, 75 %, Sigma-Aldrich), *N,N*-dimethyl-*p*-toluidine (DMT, 99 %, Sigma-Aldrich), *N,N*-dihydroxyethyl-*p*-toluidine (DHEPT, ≥ 97 %, Sigma-Aldrich) and chloroform (≥ 99 %, Sigma-Aldrich) was used without further purification. Poly(methyl methacrylate) (M_n=50.000 g/mol, M_w=100.000 g/mol) was obtained by Arkema and used as received. Methyl methacrylate (99 %, Sigma-Aldrich) inhibited with 30 ppm MEHQ was used as received.

2. Determination of BPO/DMT decomposition kinetics by HPLC

Results of HPLC in Figure S1 do not show good separation between the different reactants, BPO, DMT and dibutyl maleate. Dibutyl maleate is used as solvent for BPO, which cannot be eliminated.

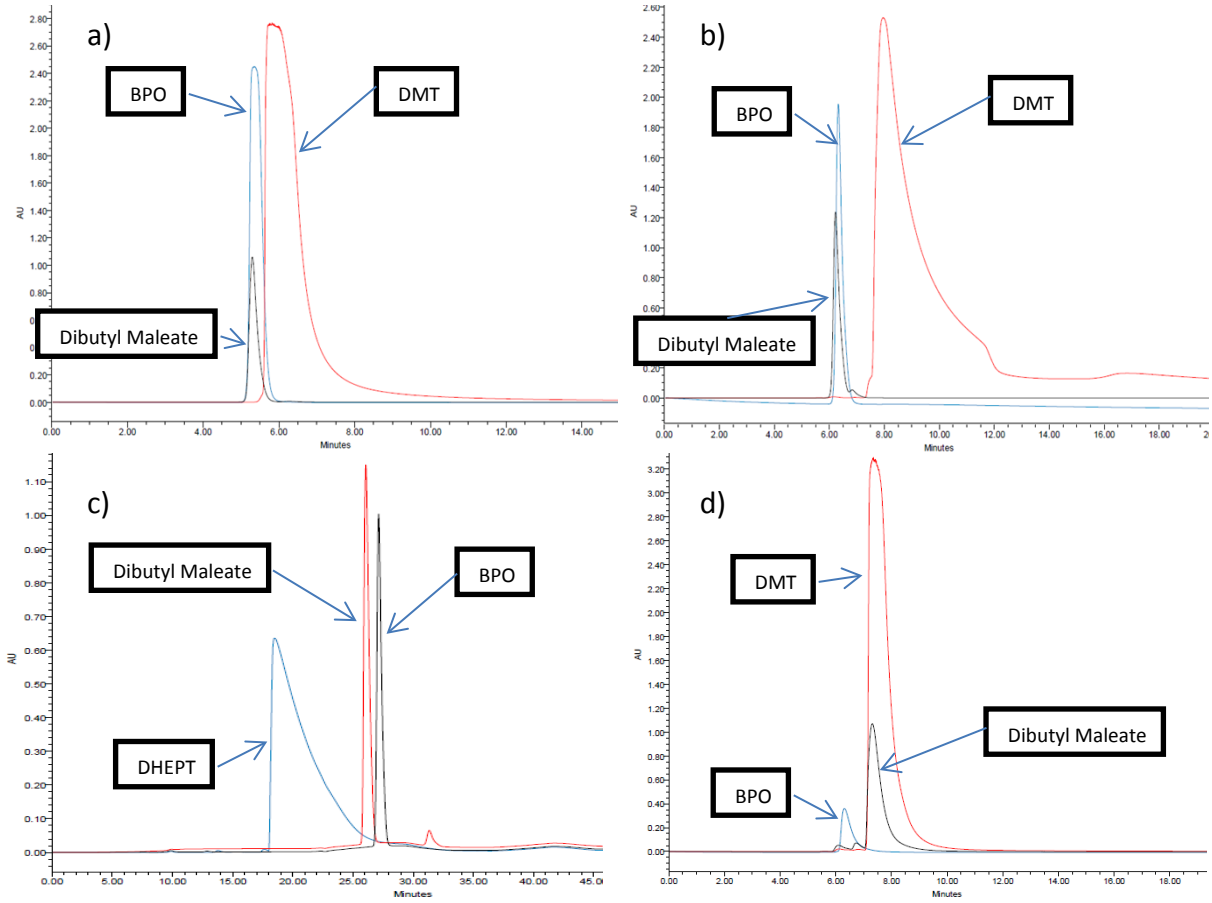

Figure S1: Elution diagram of HPLC measurements. a) BPO (blue) /DMT (red), eluent: THF, column: C18-Si; b) BPO (blue) /DMT (red), eluent: AcN, column: C18-Si; c) BPO (black) /DHEPT (blue), eluent: can-H_2O, column: C18-Si; d) BPO (blue) /DMT (red), eluant: CH_2Cl_2, column: NH_2.

3. Determination of BPO/DMT decomposition kinetics by ^{13}C-NMR

Figure S2 shows the ^{13}C-NMR spectra of BPO and DMT with the BPO and DMT signals at 164 ppm and 149 ppm respectively, which can be easily distinguished. In Figure S3 is shown the decomposition kinetics at 20 °C of the BPO/DMT reaction that is too fast to be followed by ^{13}C-NMR. Further it was tried to follow the kinetics at -20 °C in Figure S4, which shows better results than at room temperature, but the decompositions is still too fast to quantify and analyze properly the reaction rate.

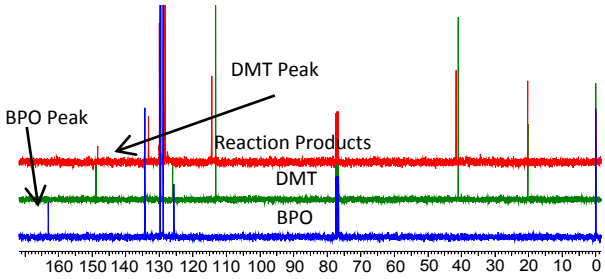

Figure S2: ^{13}C-NMR spectra of BPO and DMT.

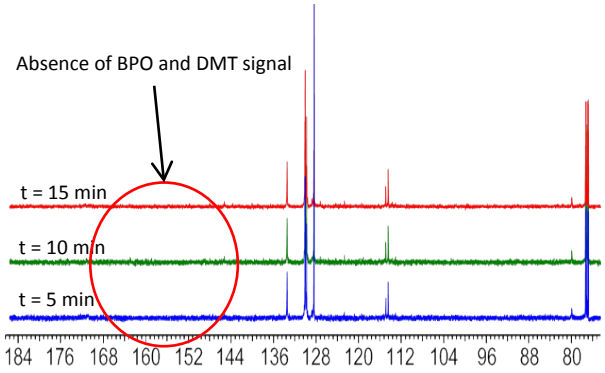

Figure S3: ^{13}C-NMR spectra of the decomposition kinetics of BPO/DMT at 20 °C.

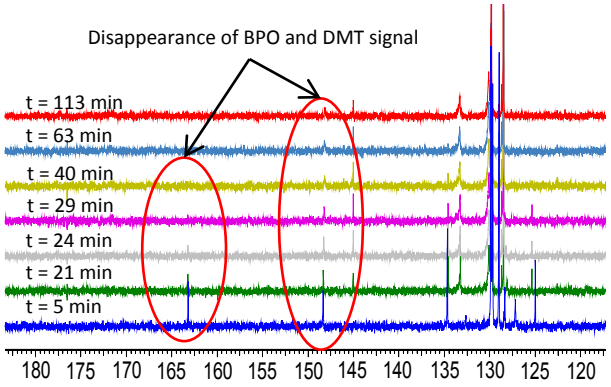

Figure S4: ^{13}C-NMR spectra of the decomposition kinetics of BPO/DMT at -20 °C.

4. Decomposition kinetics by IR-tracking

Decomposition kinetics had been measured on a Mettler Toledo ReactIR iC10. Experiments had been carried out between 0 °C and 50 °C and equimolar concentrations of BPO and amine between 0.01M and 0.1M. A chloroform solution had been thermostated in a water bath and the exact temperature was taken. BPO and amine had been dissolved separately in chloroform

as stock solution and added to the thermostated chloroform solution in order to obtain the concentration.

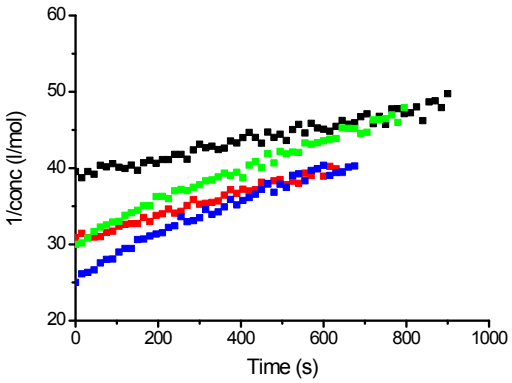

Figure S5: Decomposition kinetics BPO/DMT at 22 °C for different equimolar concentrations (0.02 mol/l black, 0.025 mol/l red, 0.05 mol/l green and 0.1 mol/l blue).

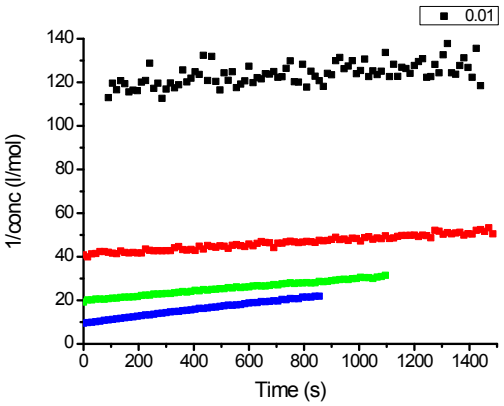

Figure S6: Decomposition kinetics BPO/DHEPT at 22 °C for different equimolar concentrations (0.01 mol/l black, 0.025 mol/l red, 0.05 mol/l green and 0.1 mol/l blue).

5. Polymerization kinetics of MMA with BPO/tertiary amine initiator

BPO (0.25 mol% - 1.5 mol%) was dissolved in MMA (0.1 mol) and degassed with argon for 10 min. The amine (DHEPT dissolved in MMA or pure DMT) was added in equimolar concentration with respect to BPO to the solution and the temperature profile was recorded by using a pico TC-08 data logger and type K thermocouple.

6. NMR analysis

NMR analysis was performed on a Bruker Avance III 400MHz Nanobay spectrometer. H-NMR spectra had been recorded at 300 K with a 12.7 µs pulse and a repetition time of 2 s and 128 scans. Deuterated chloroform ($CDCl_3$, 99.9 % D, euriso-top) was used as solvent. Conversion was calculated by the following formula

$$X(\%) = \frac{I\,(-CH-CH_2-)}{I(CH=CH_2) + I(-CH-CH_2-)} = \frac{I\,(1.02\,ppm) + I\,(0.85\,ppm)}{I\,(6.10\,ppm) + I\,(5.55\,ppm) + I\,(1.02\,ppm) + I\,(0.85\,ppm)}$$

7. SEC analysis

SEC experiments were performed on an EcoSEC from PSS, which is equipped with a dual flow cell refractive index (RI) detector. THF was used as eluent at a flow rate of 0.3 ml/min for the sample pump and 0,15 ml/min for the reference pump. The stationary phase was a combination of one PL Resipore (50 mm x 4.6 mm) guard column and two PL Resipore (250 mm x 4.6 mm) columns thermoregulated at 40 °C. Samples were prepared at a concentration of about 0.25 wt% in THF containing 0.25 vol% toluene as flow marker. The injection volume was 20 ml. Polystyrene equivalent number-average molar masses (M_n) and dispersities Đ were calculated by means of PS calibration curve using PS-M Easivial standards from Agilent.

8. Influence of side-reactions

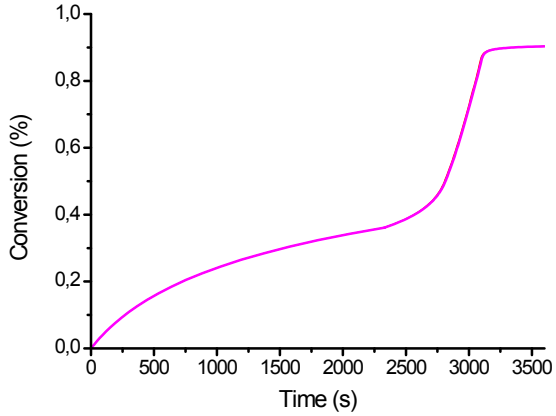

Figure S7: Conversion rate vs. time with all reaction steps (black line), without transfer to monomer (red line) and without termination by initiator (pink line).

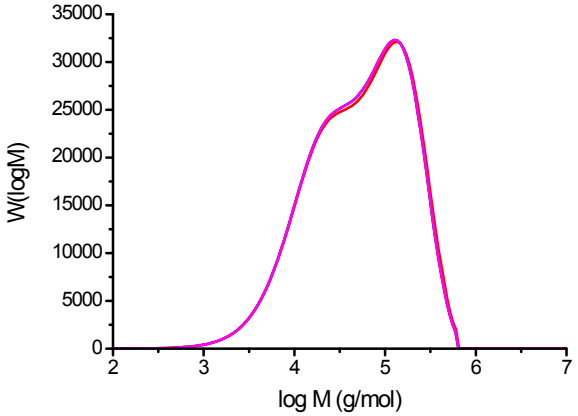

Figure S8: SEC data with all reaction steps (black line), without transfer to monomer (red line) and without termination by initiator (pink line).

9. Bimodal Molecular Weight Distribution (MWD)

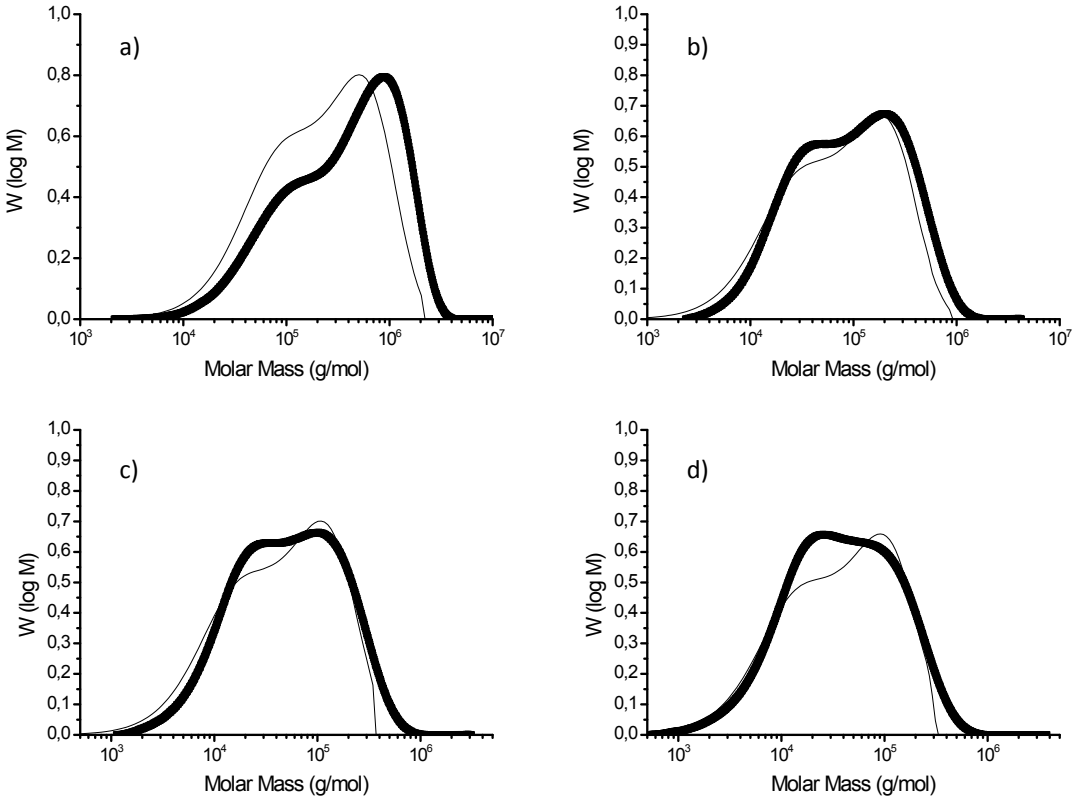

Figure S9: Modeled (thin line) and measured SEC data (thick line) from MMA polymerization with different equimolar concentrations of BPO/DMT. a) 0.25 mol%; b) 0.75 mol%; c) 1.25 mol%; d) 1.5 mol%.

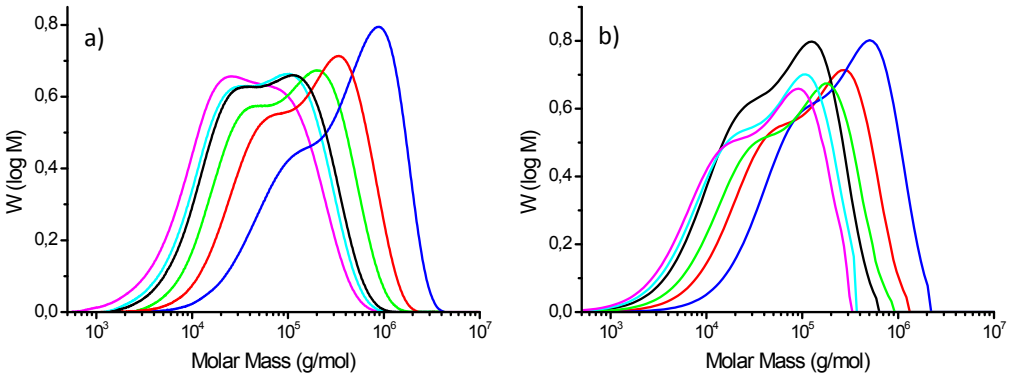

Figure S10: SEC data (a) and simulated SEC data (b) for different initiator concentrations of BPO/DMT (1.5 mol% pink, 1.25 mol% light blue, 1 mol% black, 0.75 mol% green, 0.5 mol% red, 0.25 mol% blue).

10. MMA polymerization with BPO/DHEPT

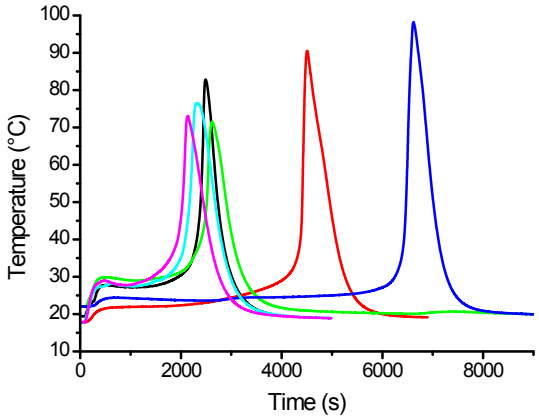

Figure S11: Temperature curves vs. time for different initiator concentrations of BPO/DHEPT (1.5 mol% pink, 1.25 mol% light blue, 1 mol% black, 0.75 mol% green, 0.5 mol% red, 0.25 mol% blue).

11. PMMA/MMA syrup polymerization with BPO/DHEPT

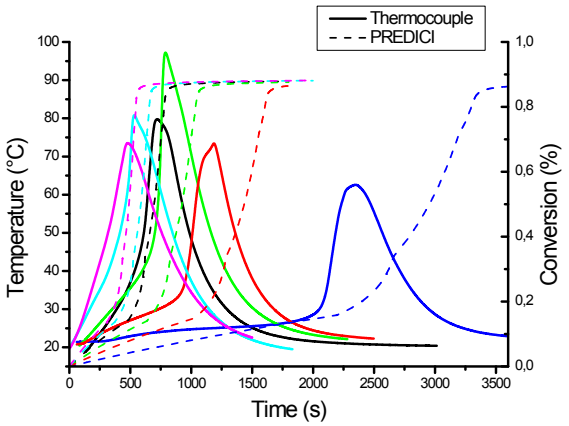

Figure S12: Temperature (straight line) vs. Simulated conversion (dotted line) profile of different initiator concentrations (1.5 mol% brown, 1.25 mol% light blue, 1 mol% black, 0.75 mol% pink, 0.5 mol% blue, 0.25 mol% red) in 75/25 MMA/PMMA syrup.

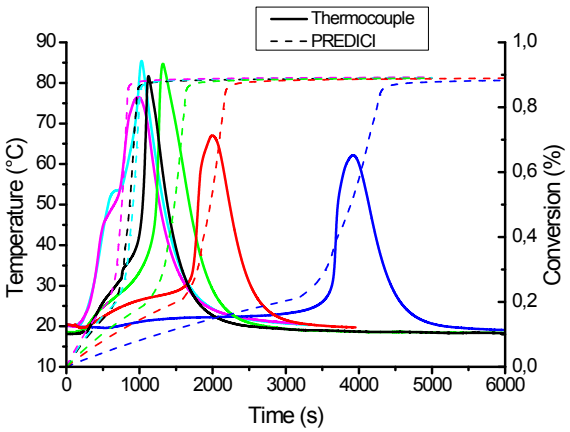

Figure S13: Temperature (straight line) vs. Simulated conversion (dotted line) profile of different initiator concentrations (1.5 mol% pink, 1.25 mol% light blue, 1 mol% black, 0.75 mol% green, 0.5 mol% red, 0.25 mol% blue) in 80/20 MMA/PMMA syrup.

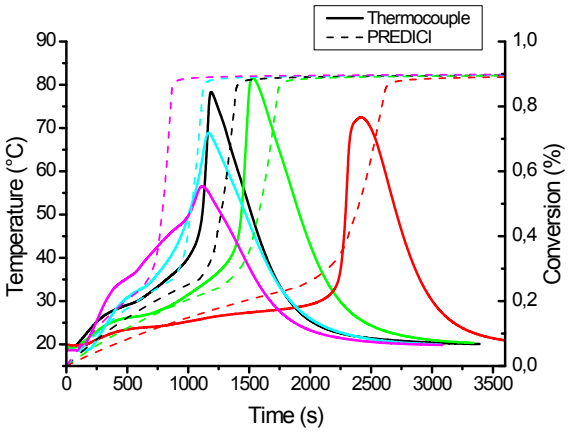

Figure S14: Temperature (straight line) vs. Simulated conversion (dotted line) profile of different initiator concentrations (1.5 mol% pink, 1.25 mol% light blue, 1 mol% black, 0.75 mol% green, 0.5 mol% red) in 85/15 MMA/PMMA syrup.

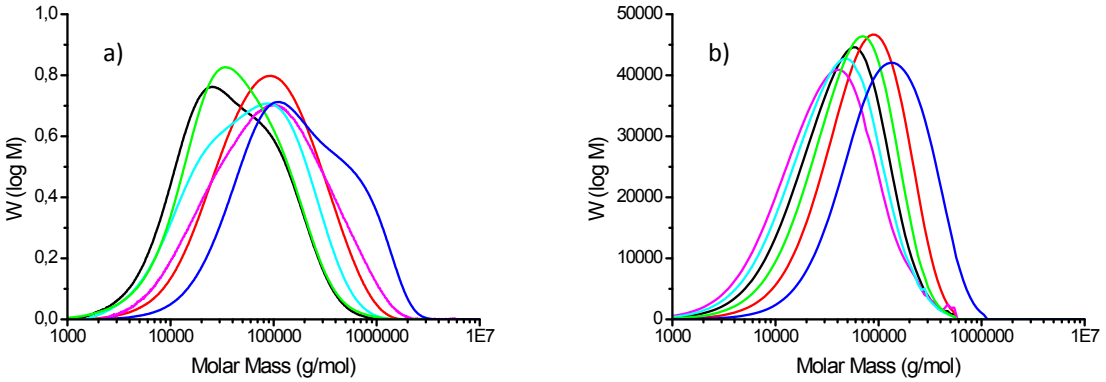

Figure S15: Molar Mass Distribution of different initiator concentrations (1.5 mol% pink, 1.25 mol% light blue, 1 mol% black, 0.75 mol% green, 0.5 mol% red, 0.25 mol% blue) with SEC (a) and Simulation (b) in 75/25 MMA/PMMA syrup.

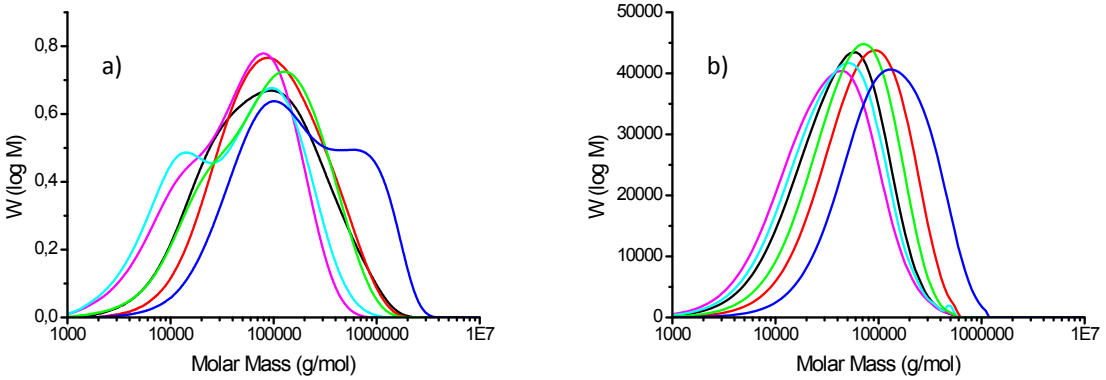

Figure S16: Molar Mass Distribution of different initiator concentrations (1.5 mol% pink, 1.25 mol% light blue, 1 mol% black, 0.75 mol% green, 0.5 mol% red, 0.25 mol% blue) with SEC (a) and Simulation (b) in 80/20 MMA/PMMA syrup.

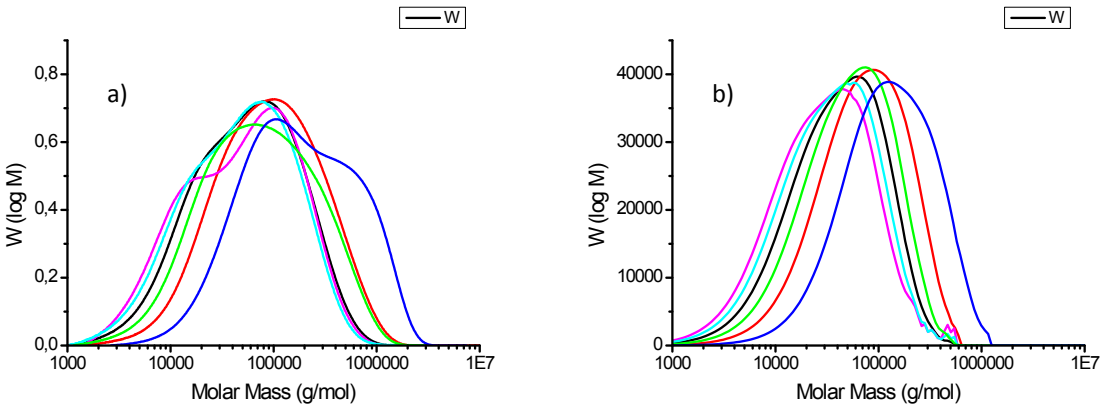

Figure S17: Molar Mass Distribution of different initiator concentrations (1.5 mol% pink, 1.25 mol% light blue, 1 mol% black, 0.75 mol% green, 0.5 mol% red, 0.25 mol% blue) with SEC (a) and Simulation (b) in 85/15 MMA/PMMA syrup.

Table S1: Comparison of experimental polymerization time and molar mass distribution measured by SEC and modelled polymerization time and SEC data for 75 % MMA and 25 %PMMA.

Initiator Concentration mol %	$t_{T,max}$ of Polymerization s	PREDICI On-Set time s	PREDICI End of Polymerization s	M_n - SEC g/mol	M_w - SEC g/mol	M_n - PREDICI g/mol	M_w - PREDICI g/mol
0.25	2350	2400	3300	82500	355900	65900	166000
0.5	1200	1100	1600	34900	82800	41100	98600
0.75	815	700	1050	28200	95600	29600	75100
1	675	540	780	18600	64850	23000	63800
1.25	620	430	650	29500	121700	19000	56300
1.5	570	350	550	65500	216800	16200	53500

Table S2: Comparison of experimental polymerization time and molar mass distribution measured by SEC and modelled polymerization time and SEC data for 80 % MMA and 20 %PMMA.

Initiator Concentration mol %	$t_{T,max}$ of Polymerization s	PREDICI On-Set time s	PREDICI End of Polymerization s	M_n - SEC g/mol	M_w - SEC g/mol	M_n - PREDICI g/mol	M_w - PREDICI g/mol
0.25	3000	3500	4250	75300	372100	68300	186100
0.5	1300	1600	2150	41100	135100	40800	106000
0.75	1550	1400	1800	34700	151200	30500	80800
1	800	800	1050	22600	84900	22100	64300
1.25	930	750	1000	17000	88100	19400	57900
1.5	880	650	850	18700	77000	16400	50900

Table S3: Comparison of experimental polymerization time and molar mass distribution measured by SEC and modelled polymerization time and SEC data for 85 % MMA and 15 %PMMA.

Initiator Concentration mol %	$t_{T,max}$ of Polymerization s	PREDICI On-Set time s	PREDICI End of Polymerization s	M_n - SEC g/mol	M_w - SEC g/mol	M_n - PREDICI g/mol	M_w - PREDICI g/mol
0.25	5100	4500	5250	80450	333550	67000	190000
0.5	2420	2200	2600	39950	114250	38000	105500
0.75	1600	1500	1800	28200	95600	26700	76700
1	1300	1200	1500	18600	64850	20500	62100
1.25	1100	1000	1300	28200	111200	16700	54400
1.5	1100	800	1000	53100	195650	14200	50200

12. Model Development

Figure S18 shows the polymerization model of MMA initiated by a decomposition reaction of BPO and a tertiary amine. After decomposition, the amine and benzoyloxy radicals initiate the polymerization reaction. Termination occurs by recombination and disproportion, whereat for MMA polymerization, the disproportion is more important.[1] Several side reactions occurring during polymerization of MMA and taken into account for the model are transfer reactions to the amine and peroxide initiator, transfer reactions to the monomer and termination reactions by amine and benzoyloxy radicals.

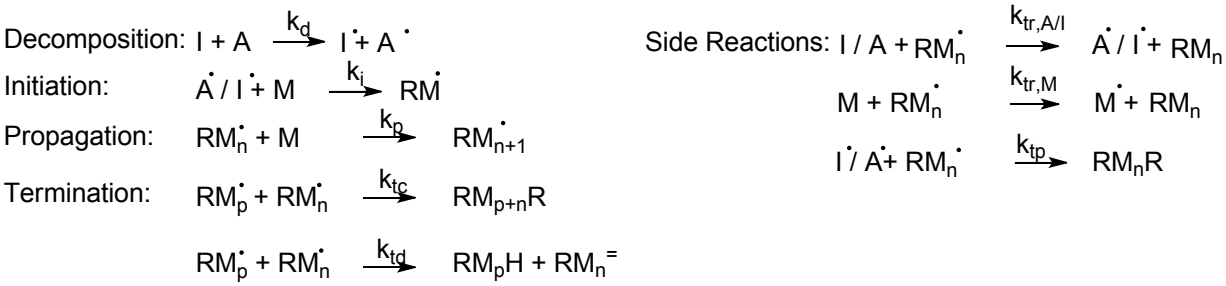

Figure S18: Scheme of a "bicomponent" Free Radical Polymerization (FRP) with I=Initiator, A=Amine, R=Decomposition Component, M=Monomer, radicals are denoted with a dot.
In the following sections the details of the different model steps are explained.

12.1 Decomposition and Initiation

The classical initiation mechanism for FRP is either a thermal decomposition reaction or photoinitiation by UV-Vis irradiation. In this study the decomposition mechanism is a bicomponental reaction between BPO and a dimethylaniline (DMA) derivative, where the DMA derivative acts as an activator for BPO. In order to complete the model, thermal decomposition was considered as well even though it has very little influence on the radical concentration at that temperature.

The efficiency of the initiation reaction is very important for modelling polymerization reactions. Achilias et al. propose a model for the initiator efficiency which is based on the free volume theory.[2,3]

$$f = \frac{f_0}{1 + \frac{C}{D_I}}, with\ D_I = D_{I0}\ exp(-\frac{\gamma_I}{V_f}) \quad (1)$$

The parameters are defined as follows: C is an adjustable parameter and D_I the radical diffusion coefficient with γ_I as overlapping factor of the radical and V_f the free volume. The free volume V_f will be developed in the section about the propagation rate.

The initiation reaction between radical and first MMA monomer is kept constant over the whole polymerization range.

12.2 Propagation

An IUPAC working party on "Modeling of kinetics and processes of polymerization"[4] analyzed the data of the propagation rate coefficients in bulk polymerization of MMA at low conversion coming from different laboratories. It was evaluated for a temperature range between 0 °C and 90 °C by pulsed-laser polymerization coupled with molar mass distribution (PLP-MMD). The following Arrhenius equation is recommended by IUPAC[4]

$$k_p = 2.67 \times 10^6 \frac{l}{mol \times s} exp(-\frac{22360 \frac{J}{mol}}{RT}) \quad (2)$$

From literature it is known that the propagation rate for polymerizations stays constant up to the glassy state mostly at a conversion of about 80-90 % as shown in Figure S19. By then the propagation reaction becomes diffusion controlled. In the case of MMA polymerization it was shown by different research groups that no decrease with conversion was observed for low and intermediate conversion. However, near the glass transition at a conversion of about 80 %, k_p begins to drop rapidly.[5–7]

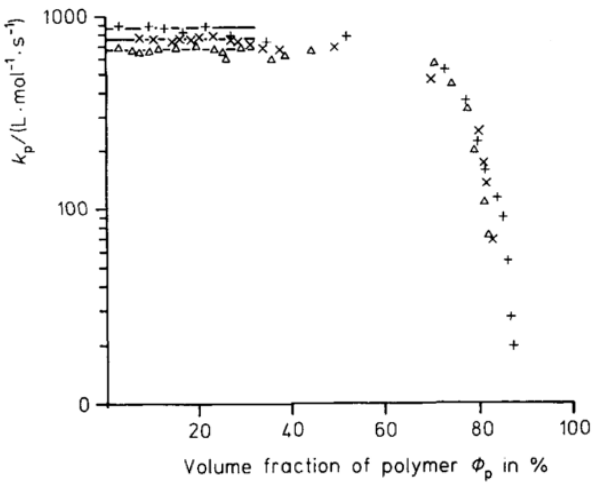

Figure S19: Propagation rate k_p for MMA bulk polymerization vs. monomer conversion.[5]

Achilias et al. developed a diffusion model based on the free-volume theory. The original model was used for a cross-linking system of dimethacrylate monomers[3], but was also presented for general MMA bulk polymerization[8]. The proposed equation is as follows

$$\frac{1}{k_p} = \frac{1}{k_{p,0}} + \frac{1}{4\pi N_A r_p D_m} \tag{3}$$

with the propagation rate constant at low conversions $k_{p,0}$, the Avogadro constant N_A, the diffusion coefficient of MMA D_m and the effective reaction radius r_p which is calculated by half of the Lennard-Jones diameter σ.[9] The Lennard-Jones-diameter is the distance from the molecule where the sum of attraction and repulsion is zero.

$$r_p = \frac{\sigma}{2} \tag{4}$$

The term $4\pi N_A r_{AB} D_{AB}$ in equation (3) is taken from the Smoluchowski equation[10], which describes the diffusion-controlled reaction between two particles. The assumption of $D_{AB} = D_m$ is made as the diffusion of the monomer is much faster than that of the polymer.

The monomer diffusion is then calculated by

$$D_m = D_{m,0} exp(-\frac{\gamma_m}{V_f}) \tag{5}$$

where $D_{m,0}$ is a preexponential factor and γ_m the overlapping factor depending on the size of the molecule. V_f is the fractional free volume which is calculated by

$$V_f = V_{f,m}(1 - \varphi_p) + V_{f,p}\varphi_p \tag{6}$$

with

$$V_{f,m} = V_{g,m} + \alpha_m(T - T_{g,m}) \tag{7}$$

$$V_{f,p} = V_{g,p} + \alpha_p(T - T_{g,p}) \tag{8}$$

$$\varphi_p = \frac{x(1 - \varepsilon_v)}{1 - x\varepsilon_v} \tag{9}$$

The notations, with the subscripts p and m for polymer and monomer respectively, refer to the volume expansion coefficient α, the free volume at the glass transition V_g, the volume fraction of the polymer φ, the reaction temperature T, the glass transition temperature T_g, the monomer conversion x and the volume contraction factor ε calculated by

$$\varepsilon_v = \frac{\vartheta_m - \vartheta_p}{\vartheta_m} \tag{10}$$

with ϑ as the specific volume.

In the model as presented above, volume relaxation effects occurring during polymerization are not taken into account. There are several other models in which these effects had not been taken into account.[2,11,12]

The diffusion of MMA during bulk polymerization was studied by Karlsson et al.[13] These results, which are shown in Figure S20, had been compared to the diffusion of the monomer Dm applied in the model. The literature values had been measured at 50 °C, so that the model was put to the same temperature for modelling the diffusion coefficient of the monomer.

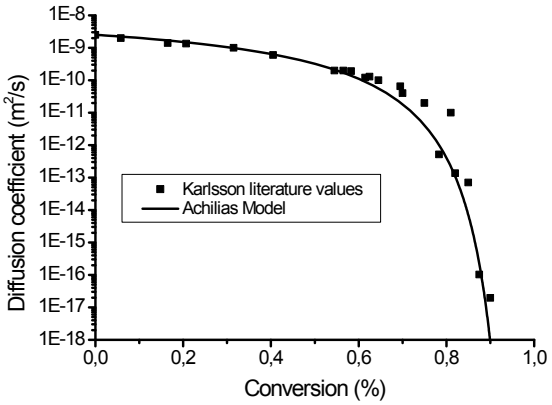

Figure S20: Experimental diffusion coefficient of MMA vs. modeled diffusion coefficient at 50 °C.

12.3 Termination

The termination rate constant k_t shows mainly four different regions during the polymerization. The first region is dominated by segmental diffusion, where k_t stays almost constant. In the second region the termination rate decreases rapidly as the viscosity increases during the gel effect. Region three has a constant low termination rate where the motion of the polymer becomes very slow and the movement is due to monomer addition at the chain ends. In the last region, k_t declines sharply again due to the glass effect.

The IUPAC working group "Modeling of Polymerization Kinetics and Processes"[14] is working on the evaluation of termination rate coefficients. They stated that due to the strong dependency on the polymerization system (chain length, conversion, viscosity, temperature etc.); it is very difficult to compare and to obtain termination rate coefficients that can be used for different systems. Therefore an empirical termination model proposed by Russell et al. describing the different conversion areas was used.[9] Originally it was fitted to data obtained from emulsion polymerization. Here, it was modified from different equations given by Russell et al. in order to fit the termination rate coefficient to the model. The model contains four different areas with

$$x(MMA) < 0.35: k_t = k_{t,0} * (1 - x(MMA)) \quad (11)$$

$$0.35 \leq x(MMA) < 0.5: ln(k_t) = 27.5 - 35 * x(MMA) \quad (12)$$

$$0.5 \leq x(MMA) < 0.78: ln(k_t) = 15 - 10 * x(MMA) \quad (13)$$

$$0.78 \leq x(MMA) < 1: ln(k_t) = 28 - 26.6 * x(MMA) \quad (14)$$

Figure S21 shows the termination rate vs. MMA conversion for the equations (11)-(14) described above.

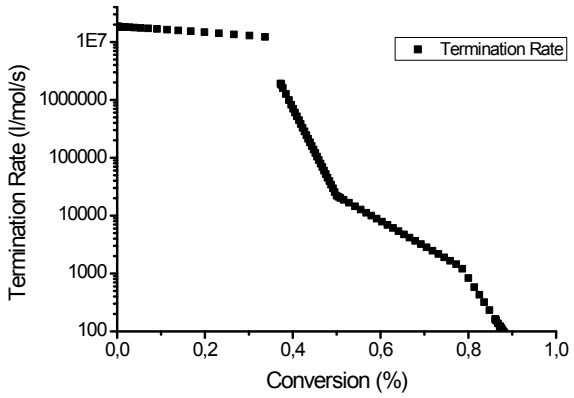

Figure S21: Empirical termination rate k_t vs. MMA conversion.

The advantage of empirical methods is the good fitting to measured data. On the other hand it becomes difficult when either the measured data is not accurate or as well when reaction kinetics changes from one system to another.

12.4 Side Reactions

During a polymerization not only decomposition, initiation, propagation and termination reactions occur but also several side reactions. The reactions shown in Figure S22 are taken into account, as there are termination reactions between radicals from the initiator and the growing polymer and chain transfer to the monomer as well as to the initiator.

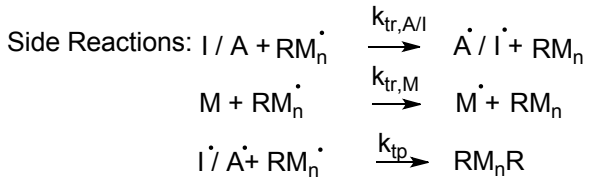

Figure S22: Occurring side reactions during free radical bulk polymerization.

As the reactions are always between the polymer chain and a small molecule (monomer, radical of BPO/Amine), the free-volume theory from the propagation rate constant is applied as model.

The transfer to the amine initiator was described by Achilias et al.[3] with the rate constant 0.1*k_p. The value is not based on experimental data but only on model fitting. It is though not proven that firstly the reaction takes place and secondly that the constant can be applied in that way.

$$\frac{1}{k_{trA}} = \frac{1}{k_{trA,0}} + \frac{1}{4\pi N_A r_p D_m} \tag{15}$$

The chain transfer to monomer reaction should be taken into account even if it is not one of the most important phenomena occurring during MMA-polymerization. As described above, it is a reaction occurring between the monomer and the growing polymer chain and can be described by the same free volume model as the propagation reaction.

$$\frac{1}{k_{trM}} = \frac{1}{k_{trM,0}} + \frac{1}{4\pi N_A r_p D_m} \tag{16}$$

A more general and more often used representation of the transfer reaction to monomer is

$$C_M = \frac{k_{tr}}{k_p} \tag{17}$$

The problem about the transfer reaction to the monomer is that there are a lot of data available, but it is not possible to derive an Arrhenius law as can be seen in Figure S23. The data is very widespread.

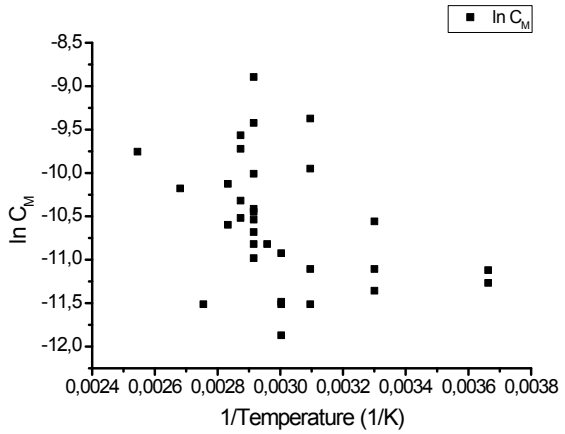

Figure S23: Transfer-to-monomer constant C_M for MMA.[15]

For modeling the parameter should be adjusted with upper and lower limits. Otherwise the influence of this reaction has to be double-checked as it is a very low number.

The reaction between initiator and the growing polymer chain is harder to describe as it is a reaction between a small radical molecule and a macroradical. The reaction is not well described in literature but it can be assumed that the reactivity must be close to that of the termination rate with the diffusivity of the chain-growth. A possible formula describing this reaction step could be

$$\frac{1}{k_{tp}} = \frac{1}{k_{tp,0}} + \frac{1}{4\pi N_A r_p D_m} \tag{18}$$

with $k_{tp,0} = k_{t,0}$ as a first approximation.

Table S4: Kinetic and physical parameters of MMA bulk polymerization initiated by BPO/amine

Kinetic Parameter	Reference	Physical Parameter	Reference
$k_{d,BPO/DMT,0}$ = 832*exp(-26 kJ/RT) l/mol/s	This work	ν_m = 1.064 ml/g	-
$k_{d,BPO/DHEPT,0}$ = 7400*exp(-33.4 kJ/RT) l/mol/s	This work	ν_p = 0.847 ml/g	-
$k_{d,BPO,0}$ = 5*10[16]*exp(-143 kJ/RT) l/mol/s	[15]	α_m = 0.001234	[16]
$f_{BPO/DMT,0}$ = 0.2	Estimated	α_p = 0.00021	[17]
$f_{BPO/DHEPT,0}$ = 0.3	Estimated	$T_{g,m}$ = -126 °C	[18]

$f_{BPO,0}$ = 0.4	[19]	$T_{g,p}$ = 114 °C	[18]
$k_{i,BPO,0}$ = 1.76*10^8 l/mol/s	[19]	$D_{m,0}$ = 0.0003 cm^2/s	Fit from [13]
$k_{i,DMT,0}$ = 9.7*10^5 l/mol/s	DMA/MA[20]	γ_m = 0.6	Fit from [13]
$k_{i,DHEPT,0}$ = 9.7*10^5 l/mol/s	DMA/MA[20]	γ_I = 0.41	[3]
$k_{p,0}$ = 2.67*10^6*exp(-22.36 kJ/RT) l/mol/s	[4]	σ = 0.585 nm	[21]
$k_{t,0}$ = 1.984*10^8*exp(-5.89 kJ/RT) l/mol/s	[22]	N_A = 6.022*10^{23} 1/mol	-
δ = 0.67	[23]	j_c = 70	[15]
$C_{MMA,0}$ = 0.00005	[15]	α = 0.69 nm	[24]
$C_{BPO,0}$ = 0.06	[15]	$C/D_{I,0}$ = 50000	[3]
$C_{DMT,0}$ = 0.3	Estimated		
$C_{DHEPT,0}$ = 0.15	Estimated		

References

1 C. H. Bamford, G. C. Eastmond and D. Whittle, *Polymer (Guildf).*, 1969, **10**, 771–783.

2 D. S. Achilias and C. Kipasissides, *Macromolecules*, 1992, **25**, 3739–3750.

3 D. S. Achilias and I. D. Sideridou, *Macromolecules*, 2004, **37**, 4254–4265.

4 S. Beuermann, M. Buback, T. P. Davis, R. G. Gilbert, R. A. Hutchinson, O. F. Olaj, G. T. Russell, J. Schweer and A. M. van Herk, *Macromol. Chem. Phys.*, 1997, **198**, 1545–1560.

5 J. Shen, Y. Tian, G. Wang and M. Yang, *Die Makromol. Chemie*, 1991, **192**, 2669–2685.

6 S. Zhu, Y. Tian, A. E. Hamielec and D. R. Eaton, *Macromolecules*, 1990, **1150**, 1144–1150.

7 T. G. Carswell, D. J. T. Hill, D. I. Londero, J. H. O'Donnell, P. J. Pomery and C. L. Winzor, *Polymer (Guildf).*, 1992, **33**, 137–140.

8 D. S. Achilias, *Macromol. Theory Simulations*, 2007, **16**, 319–347.

9 G. T. Russell, D. H. Napper and R. G. Gilbert, *Macromolecules*, 1988, **21**, 2141–2148.

10 M. v. Smoluchowski, *Zeitschrift für Phys. Chemie*, 1916, **XCII**, 129–168.

11 I. Hace, J. Golob and M. Krajnc, *J. Appl. Polym. Sci.*, 2005, **96**, 345–357.

12 I. Hace, J. Golob and M. Krajnc, *Polym. Eng. Sci.*, 2004, **44**, 2005–2018.

13 O. J. Karlsson, J. M. Stubbs, L. E. Karlsson and D. C. Sundberg, *Polymer (Guildf).*, 2001, **42**, 4915–4923.

14 M. Buback, M. Egorov, R. G. Gilbert, V. Kaminsky, O. F. Olaj, G. T. Russell, P. Vana and G. Zifferer, *Macromol. Chem. Phys.*, 2002, **203**, 2570–2582.

15 J. Brandrup, E. H. Immergut and E. A. Grulke, *Polymer Handbook*, Wiley-Interscience, 4 Edition., 2003.

16 S. L. Oswal, B. M. Patel, A. M. Patel and N. Y. Ghael, *Fluid Phase Equilib.*, 2003, **206**, 313–329.

17 R. Greiner and F. R. Schwarzl, *Rheol. Acta*, 1984, **23**, 378–395.

18 J. N. Cardenas and K. F. O'Driscoll, *J. Polym. Sci. Polym. Chem. Ed.*, 1976, **14**, 883–897.

19 G. Moad and D. H. Solomon, *The Chemistry of Free Radical Polymerization*, Pergamon-Elsevier Science Ltd., Oxford, 2nd Editio., 1995, vol. 109.

20 J. Lalevée, B. Graff, X. Allonas and J. P. Fouassier, *J. Phys. Chem. A*, 2007, **111**, 6991–6998.

21 P. A. Clay, R. G. Gilbert and G. T. Russell, *Macromolecules*, 2006, **9297**, 1935–1946.

22 D. R. Taylor, K. Y. van Berkel, M. M. Alghamdi and G. T. Russell, *Macromol. Chem. Phys.*, 2010, **211**, 563–579.

23 K. Matyjaszewski, *Handbook of Radical Polymerization*, John Wiley & Sons, Inc., 1 edition., 2002.

24 G. T. Russell and D. H. Napper, *Macromolecules*, 1988, **21**, 2133–2140.